Environmental Science & Technology Letters

Letter

pubs.acs.org/journal/estlcu

Atmospheric Processing of Combustion Aerosols as a Source of Bioavailable Iron

Akinori Ito*

Yokohama Institute for Earth Sciences, JAMSTEC, Yokohama, Kanagawa 236-0001, Japan

Supporting Information

ABSTRACT: Atmospheric processing of combustion aerosols may promote transformation of insoluble iron into soluble forms. Here, an explicit scheme for iron dissolution of combustion aerosols due to photochemical reactions with inorganic and organic acids in solution is implemented in an atmospheric chemistry transport model to estimate the atmospheric sources of bioavailable iron. The model results suggest that deposition of soluble iron from combustion sources contributes more than 40% of the total soluble iron deposition over significant portions of the open ocean in the Southern Hemisphere. A sensitivity simulation using half the iron dissolution rate for combustion aerosols results in relatively small decreases in soluble iron deposition in the ocean, compared with the large uncertainties associated with iron solubility at emission. More accurate quantification of the soluble iron burdens near the source regions and the open ocean is needed to improve the process-based understanding of the chemical modification of iron-containing minerals.

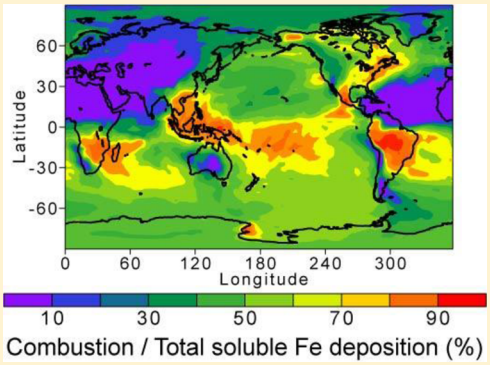

INTRODUCTION

The majority of bioavailable iron (Fe) from the atmosphere is delivered from arid and semiarid regions to the oceans because the global deposition of iron from combustion sources is small compared with that from mineral dust.[1,2] Recently, global three-dimensional (3D) atmospheric transport model studies have emphasized the large uncertainties in the spatial distribution of soluble iron deposition due to combustion-derived aerosols.[3−6] Iron-containing aerosols that are influenced by air masses from anthropogenic sources are often observed to have high iron solubilities (soluble Fe/total Fe).[1,7,8] The iron solubilities observed for aerosols that are influenced by biomass burning vary by 2 orders of magnitude from 0.5 to 46%.[1,9,10] Field observations have further suggested that high iron solubility is likely associated with high oxalate concentrations due to anthropogenic emission sources.[11,12] Moreover, laboratory studies have demonstrated that the iron solubilities of combustion-derived aerosols are substantially greater than those of crystalline minerals.[13−15] The iron species within combustion aerosols play a crucial role in controlling the iron solubility of aerosols, as discussed below and in previous studies.[6,8,10−16] Furthermore, the results of laboratory experiments have suggested that ligand-promoted dissolution of iron may play a more significant role in the transformation of insoluble iron to soluble forms than proton-assisted processing.[16] These studies highlight the importance of organic compounds for iron mobilization, but the dissolution of iron from combustion aerosols has not been explicitly simulated in modeling studies.

Here, a global chemical transport model is used to investigate the effect of atmospheric processing of combustion aerosols on iron mobilization. This study incorporates an explicit iron dissolution scheme for the combustion aerosols in our model,[17] which is based on laboratory experiments.[14−16] In previous studies, we used the model to investigate the factors associated with the uncertainty in soluble iron deposition due to variations in the dust alkalinity,[18] intensity of forest fires,[4] iron solubility in biomass burning aerosols,[5] dust size distribution,[19] iron solubility of combustion aerosols,[6] and mineralogy of the dust aerosols.[17] An updated version of the model has been used to estimate the formation of oxalate in the water shell of aerosols and cloud droplets.[20,21] The effects of iron mobilization on atmospheric mineral materials from oil combustion, biomass burning, and coal combustion are explored.

METHODOLOGY

In our model, iron dissolution from aerosols due to chemical processing is calculated on the basis of an online simulation of aqueous-phase chemistry.[5,17,18] Laboratory studies have demonstrated that the dissolution rate of minerals is dependent on the proton concentration in bulk solution, the mineral surface concentration of oxalate, and the temperature.[22−25] The oxalate-promoted dissolution is controlled by the release of absorbed complexes via the breaking of Fe−O bonds at the mineral surface.[22] The results of laboratory experiments regarding the release of iron over time have demonstrated that the dissolution rate increases significantly as the pH

Received: October 30, 2014
Revised: January 28, 2015
Accepted: February 2, 2015
Published: February 2, 2015

DOI: 10.1021/acs.estlett.5b00007
Environ. Sci. Technol. Lett. 2015, 2, 70−75

decreases from 3 to 2.[16] Thus, the amount of absorbed complex also increases in more acidic solutions.[22] At low oxalate concentrations in acidic solutions, dissolved Fe(III) effectively competes with the surfaces of the particles for oxalate through the formation of Fe(III)−oxalate complexes {i.e., $[Fe(C_2O_4)]^+$}, thereby suppressing surface complexation.[16] The rate is independent of the pH for extremely acidic solutions (pH <2).[14] On the basis of these studies, iron dissolution from combustion aerosols is treated explicitly as a kinetic process that depends on the pH, ambient temperature, and competition for oxalate between surface iron and dissolved iron (Table S1 of the Supporting Information). The Fe dissolution rates (RFe_{ij} in units of moles of soluble iron per gram of mineral particle per second) for each dissolution scheme i and for each iron-containing mineral j can be empirically described using the following equation, which is similar to the formulation applied for iron-containing minerals:[17,22−26]

$$RFe_{i,j} = NFe \times K_i(T) \times a(H^+)^{mi} \times f_i \times A_j \times W_j \quad (1)$$

where NFe is the stoichiometric number of moles of Fe per mole of iron oxide (NFe = 2), K_i is the temperature (T)-dependent reaction coefficient (moles per square meter per second), $a(H^+)$ is the H^+ activity, m_i represents the empirical reaction order for protons, f_i accounts for the suppression of mineral dissolution, A_j is the specific surface area of the mineral (square meters per gram), and W_j is the weight fraction of the mineral in the total mineral particle in units of grams of mineral per gram of mineral particle. The function f_i ($0 \le f_i \le 1$; R^2 = 0.99) for ligand-promoted and photoreductive dissolution is given by

$$f_i = 0.17 \times \ln(a_{lig} \times a_{Fe}{}^{-1})_i + 0.63 \quad (2)$$

where a_{Fe} is the concentration of Fe(III) dissolved in solution and a_{lig} is the concentration of ligand (e.g., oxalate). The parameters in eqs 1 and 2 are fit to the experimental data for coal fly ash.[16] The photoinduced dissolution rate is calculated by scaling the photolysis rate of H_2O_2 estimated in the model. The consumption of oxalate due to photolysis of iron−oxalate complexes[27] is simulated in aqueous chemistry.[20]

A comparison of the iron solubilities after 48 h under dark and irradiation conditions due to proton-promoted, oxalate-promoted, and photoinduced dissolution is shown in Figure S1 of the Supporting Information. The calculations reproduce the enhancement of the iron solubility due to the effects of oxalate and sunlight under acidic conditions, compared with proton-promoted dissolution. The iron solubility at pH 2, including the oxalate under dark condition, is 4 times greater than that for proton-promoted dissolution.[16] Compared with dark dissolution, photoinduced dissolution doubles the iron solubility.[16] The calculations also reproduce the suppression of oxalate-promoted iron dissolution under acidic conditions (Figure S2 of the Supporting Information). The calculated total dissolved Fe concentration (0.6 mM) after 48 h in the acidic solution (pH 2) that contains less oxalate (0.1 mM) is half of the amount in the solution (1.2 mM) that contains more oxalate (2 mM). As demonstrated by laboratory experiments, for highly acidic conditions, the amount of iron dissolved from mineral dust is also enhanced by oxalate-promoted and photoinduced dissolution.[16] However, greater pH values (>3) are typical for mineral dust and cloudwater.[5,17,18,20] Thus, the faster dissolution scheme primarily works for wet combustion aerosols during atmospheric transport, which is consistent with observations.[12]

The iron dissolution scheme is implemented in the integrated massively parallel atmospheric chemical transport (IMPACT) model (see Tables S2 and S3 and Figure S3 of the Supporting Information).[19−21,28−32] Three sensitivity simulations were performed to explore the effects of the uncertainties associated with the two equations for iron solubility. The dissolution experiments performed for three fly ash samples exhibited a wide range of increases in iron solubility, from approximately 20% (from 55% after an initial period of rapid dissolution to 78% for another sample) to approximately 40% over 45 h of acidic processing.[16] A linear correlation analysis indicated that the total dissolved iron was moderately correlated (R = 0.74) with the Fe(III) in the aluminosilicates and was weakly correlated (R = 0.13) with the Fe(III) in the oxides, which suggested that iron speciation within combustion aerosols might play a major role in controlling Fe dissolution.[16] A weak correlation (R = 0.27) between the total dissolved iron and specific surface area, which was determined using Brunauer, Emmett, and Teller (BET) analysis,[16] was also found. The reactive surface area for the Fe dissolution reaction is likely limited to small fractions of the BET surface area.[33] To evaluate the uncertainties in the dissolution rates, half of the Fe dissolution rate was used in a sensitivity simulation for combustion aerosols. After 12 h at pH 2, the iron solubility due to proton-promoted dissolution is in the range of 1.2−2.4%, which is comparable to that observed for different coal fly ash samples (2.9, 3.9, and 4.2%).[15] The differences in iron solubility observed in different samples are primarily related to the differences in the amounts of Fe that are rapidly released into solution.[14,15] These differences in the initial iron solubilities of different aerosols have been discussed in previous modeling studies.[5,6]

Suppression of the iron dissolution rate is applied to the model-calculated oxalate concentration. In our model, oxalic acid is assumed to remain entirely in the particulate phase when the water is evaporated. This behavior can be explained by the formation of stable complexes (e.g., calcium oxalate),[34] which might reduce the availability of oxalate for iron−oxalate complexes under higher-pH conditions. In contrast, our model significantly underestimates the high oxalate concentrations near sources of fossil fuel combustion and biomass burning, possibly because of the lack of rapid formation processes.[20] To isolate the effects of oxalate on iron dissolution, additional simulations are performed for two cases (f_i = 0, and f_i = 1).

RESULTS AND DISCUSSION

The model-calculated concentrations of iron and soluble iron in aerosols were extensively compared with field observations.[5,6,17,18] The daily averaged, model-calculated surface concentrations of iron for the fine mode were compared with the measurements at Mt. Abu in western India (Figure S4 of the Supporting Information).[35] The modeled aerosol iron concentration exhibits a temporal variability that is similar to that of the measurements, with relatively low values occurring during the winter months (50−600 ng m^{-3}) compared with those during the summer season (150−1000 ng m^{-3}). The contribution of combustion aerosols with low iron loading to the $PM_{2.5}$ mass is relatively large during the winter months (50%) compared with the summer season (15%). It is not straightforward to compare the daily mean of the iron oxidation

DOI: 10.1021/acs.estlett.5b00007
Environ. Sci. Technol. Lett. 2015, 2, 70−75

state of the aerosols because of its considerable variation with the amount of incoming radiation due to the fast photochemical redox cycling between Fe(III) and Fe(II) in solution.[36] Clearly, more work is required to establish the chemical forms of soluble iron. This study focuses on "potentially" bioavailable iron, which includes ferrihydrite colloids, nanoparticles, and aqueous species. In this context, the model-calculated iron solubility (7 ± 2%) is in good agreement with the measurement (8 ± 4%) during winter, when the advective transport of pollutants from northern India results in an enhancement of the iron solubility.[35]

The globally averaged depositions of soluble iron calculated in standard (sensitivity) simulations are 0.97 and 0.10 (0.07) Tg of Fe year^{-1} from dust and combustion aerosols, respectively (Table S4 of the Supporting Information). The globally averaged iron solubility for combustion aerosols in standard simulation (7.3%) is in the middle of the range of previous estimates (0.7−13%),[3] whereas the value in the sensitivity simulation (4.7%) is similar to that used for all combustion sources at emission in previous modeling studies (4%).[3,18] The contribution of combustion aerosols to the total soluble iron deposition (6 and 10%) is between the previous estimates (4−46%).[3]

The annually averaged rate of deposition of soluble iron from combustion sources to the oceans is presented in Table S5 of the Supporting Information and Figure 1a. The contributions of different aerosol types to the soluble iron deposition in global oceans are examined. Of the total deposition, 85% is from dust sources, 8.7% from biomass burning, and 6.7% from fossil fuel combustion. The globally averaged iron solubility for combustion aerosols, which is estimated from the deposition to the oceans in standard simulations, is generally consistent with that used in the previous version of our model.[6] Compared with simulations that consider only proton-promoted Fe dissolution, the addition of oxalate more than doubled the soluble iron deposition from combustion sources to global oceanic regions (Figure 1b). The dissolution rate is enhanced in excess-oxalate solutions, whereas the effect of oxalate is often suppressed near the source regions due to the low oxalate concentrations (Figure 1c). The model results are generally consistent with observations, which indicate relatively low iron solubilities near sources of biomass burning and coal combustion, such as the Mediterranean Sea and Jeju Island, Korea, and become higher as the aerosols are transported to the open ocean.[1,7,8]

The ratios of the annually averaged deposition of soluble iron from dust and each combustion aerosol to the sum of the dust and combustion aerosols are shown in Figure 2. The biomass burning sources with fast iron dissolution rates contribute significant amounts of soluble iron (40−60%) to the tropical and southern oceans downwind of Southeast Asian, South African, Australian, and South American biomass-burning sources. The larger contribution of the biomass burning aerosols in the Southern Hemisphere is associated with the higher iron solubility and smaller particle sizes of the biomass burning aerosols, in addition to fewer sources of mineral dust and fossil fuel combustion. The oil combustion sources with high iron solubilities at emission tend to contribute >30% of the total deposition of soluble iron in the high-latitude North Atlantic and North Pacific. The coal combustion sources of soluble iron are accentuated over the coastal waters downwind of East Asia, the United States, and South Africa. The soluble iron deposition from dust sources contributes less than 60% of

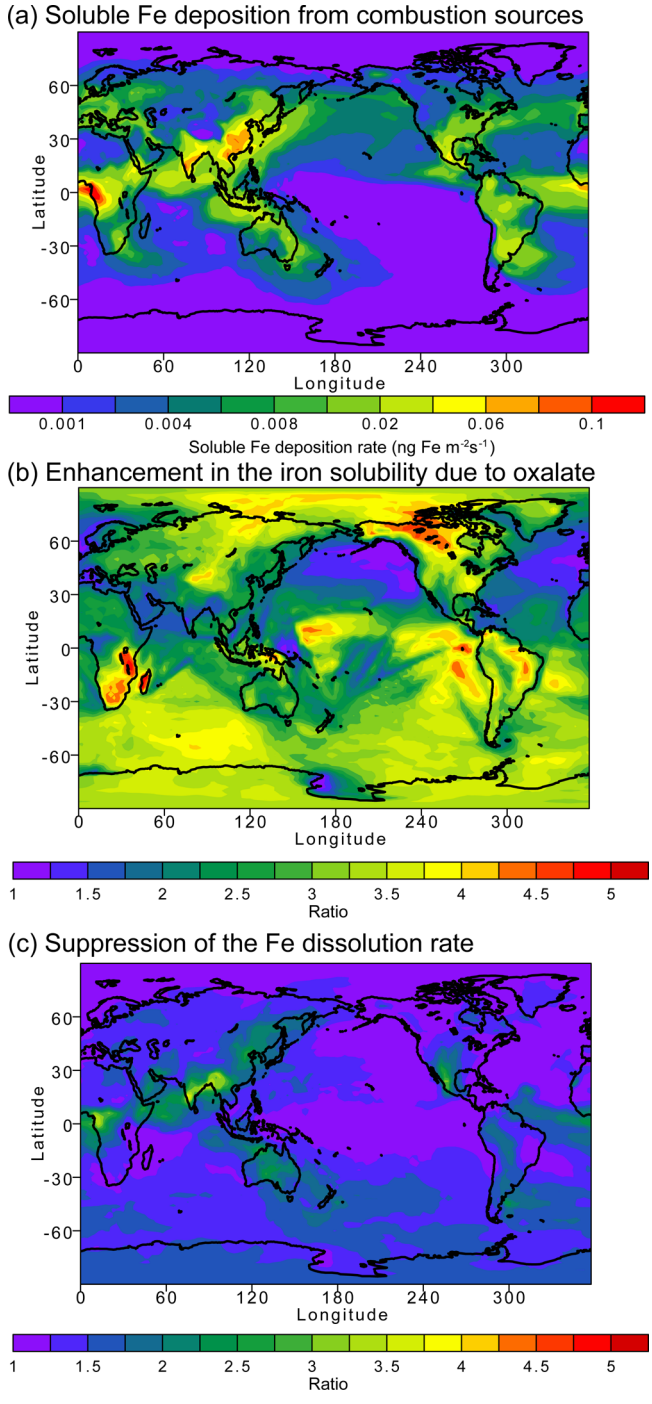

Figure 1. (a) Soluble iron deposition rate solely from combustion sources in the standard simulation (nanograms per square meter per second). (b) Ratio of soluble iron deposition from combustion sources in the standard simulation to that due solely to proton-promoted dissolution (i.e., f_i = 0 in eq 1). (c) Ratio of soluble iron deposition with no suppression effect on ligand-promoted and photoreductive iron dissolution rates (i.e., f_i = 1 in eq 1) to that in the standard simulation.

the soluble iron deposition over significant portions of the open ocean in the Southern Hemisphere.

When the iron dissolution rate used for combustion aerosols is halved, the deposition rate of soluble iron from combustion sources to the oceans decreases from 0.050 to 0.035 Tg of Fe year^{-1} (−33%). The sensitivity simulation yields a spatial

DOI: 10.1021/acs.estlett.5b00007
Environ. Sci. Technol. Lett. 2015, 2, 70−75

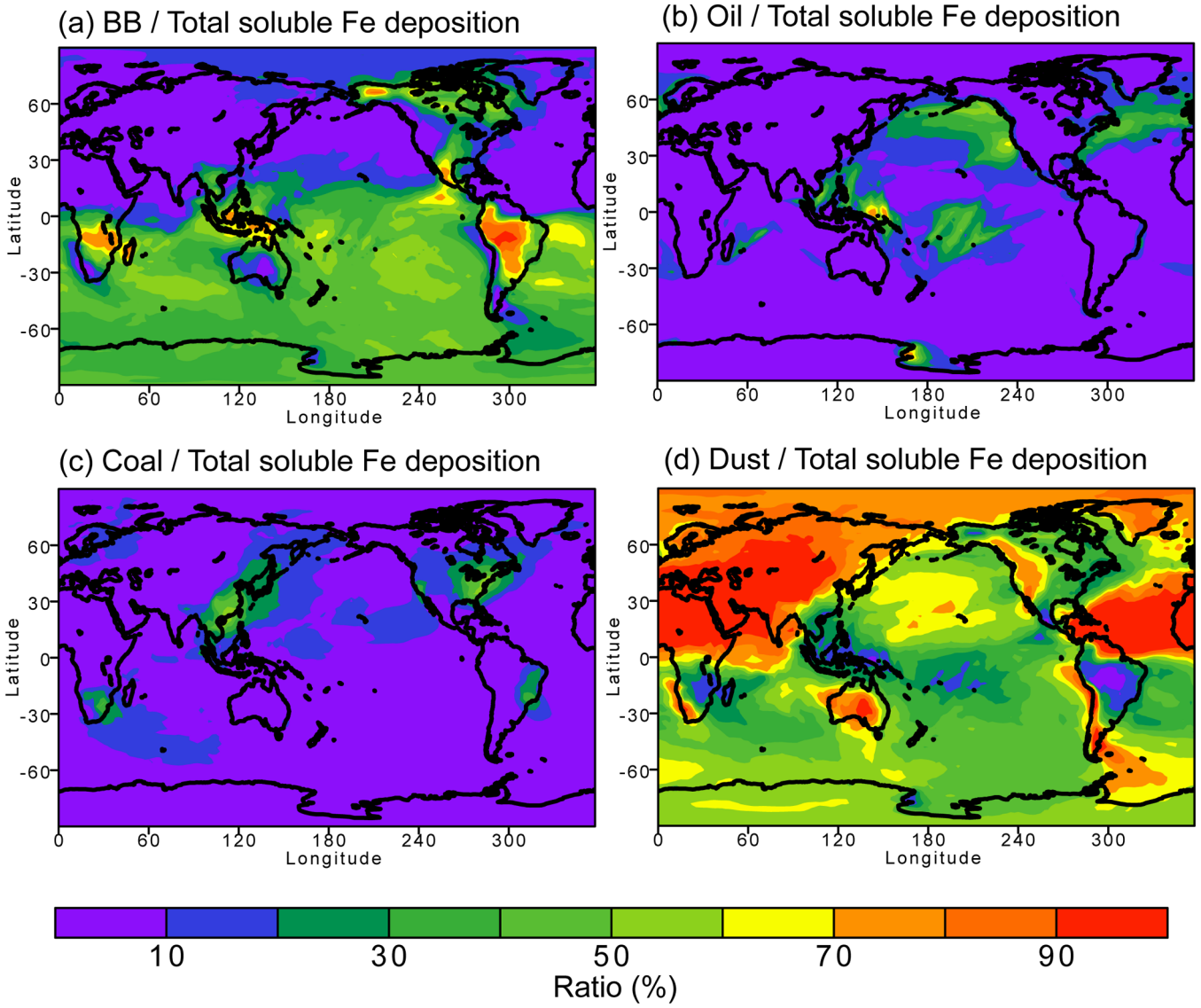

Figure 2. Contribution of each source to the total soluble iron deposition calculated in the standard simulation. (a) Ratio (%) of the soluble iron deposition solely from open biomass burning (BB) to the total soluble iron deposition. (b) Ratio (%) of the soluble iron deposition solely from oil combustion to the total soluble iron deposition. (c) Ratio (%) of the soluble iron deposition solely from coal combustion to the total soluble iron deposition. (d) Ratio (%) of the soluble iron deposition solely from dust to the total soluble iron deposition.

distribution that is similar to that of the standard simulation (Figure S5 of the Supporting Information); the differences are minor compared with the large uncertainties associated with iron solubility at emission.[5,6] In our model, high iron solubility at emission is linked to oil fly ash,[6] which contains ferric sulfate salt $[Fe_2(SO_4)_3{\cdot}9(H_2O)]$ and nanosized Fe_3O_4 aggregates.[13,15] The wide range of iron solubility observed for biomass burning aerosols may be associated with iron sulfate, amorphous forms of iron, and stable organic complexes of iron, but their formation mechanisms are not quantitatively well characterized.[10,15,37] More studies are necessary to understand the chemical forms of iron in each combustion aerosol and their relationships with the variability in bulk iron solubility.

Atmospheric deposition of soluble iron species from combustion sources may play a significant role in altering marine biological activity, depending on the region and season. The model results suggest that atmospheric processing of iron-containing minerals in wet combustion aerosols by oxalate is important for soluble iron deposition. The effects of oxalate on faster iron dissolution are suppressed because of the low oxalate concentrations near the source regions but are enhanced after cloud processing. The lack of experimental data for iron-containing minerals mixed with a variety of organic ligands in solution is an important source of uncertainty. Whereas organic ligands in the ocean may determine whether soluble iron in aerosols becomes biologically available,[38] stable organic complexes of iron can also be formed at emission and in atmospheric water.[37,39,40] The current model can represent neither the wide range of initial iron solubilities for combustion aerosols nor the reactions of iron with humic-like substances, which constitute a major fraction of the observed water-soluble organic compounds. Further field and laboratory studies are needed to determine the content of soluble iron in combustion aerosols at emission, the iron dissolution kinetics with respect to the iron speciation and reactive surface area, and the chemical forms of iron in cloudwater and aerosol water. The wide variety of organic compounds and their reactions with

DOI: 10.1021/acs.estlett.5b00007
Environ. Sci. Technol. Lett. 2015, 2, 70−75

trace metals should be incorporated into aqueous-phase chemistry modules in the future.

■ ASSOCIATED CONTENT

Supporting Information

Parameters for dissolution rates (Table S1), Fe solubility calculated from different dissolution schemes (Figure S1), dissolved Fe concentration as a function of oxalate concentration (Figure S2), emission rates (Table S2), comparison of oxalate concentrations (Table S3 and Figure S3), comparison of iron concentrations (Figure S4), deposition rates (Tables S4 and S5), and the contribution of each source to total deposition in sensitivity simulation (Figure S5). This material is available free of charge via the Internet at http://pubs.acs.org.

■ AUTHOR INFORMATION

Corresponding Author

*E-mail: akinorii@jamstec.go.jp. Phone: (+81)457785717. Fax: (+81)457785707.

Notes

The authors declare no competing financial interest.

■ ACKNOWLEDGMENTS

Support for this research was provided by Program for Risk Information on Climate Change (MEXT). All of the numerical simulations were performed using the SGI ICE X at the JAMSTEC.

■ REFERENCES

(1) Guieu, C.; Bonnet, S.; Wagener, T.; Loye-Pilot, M. D. Biomass burning as a source of dissolved iron to the open ocean? *Geophys. Res. Lett.* **2005**, *22*, L19608.

(2) Hajima, T.; Kawamiya, M.; Watanabe, M.; Kato, E.; Tachiiri, K.; Sugiyama, M.; Watanabe, S.; Okajima, H.; Ito, A. Modeling in Earth system science up to and beyond IPCC AR5. *Progress in Earth and Planetary Science* **2014**, *1*, 29.

(3) Luo, C.; Mahowald, N.; Bond, T.; Chuang, P. Y.; Artaxo, P.; Siefer, R.; Chen, Y.; Schauer, J. Combustion iron distribution and deposition. *Global Biogeochem. Cycles* **2008**, *22*, GB1012.

(4) Ito, A. Mega fire emissions in Siberia: Potential supply of bioavailable iron from forests to the ocean. *Biogeosciences* **2011**, *8*, 1679−1697.

(5) Ito, A. Contrasting the effect of iron mobilization on soluble iron deposition to the ocean in the Northern and Southern Hemispheres. *J. Meteorol. Soc. Jpn.* **2012**, *90A*, 167−188.

(6) Ito, A. Global modeling study of potentially bioavailable iron input from shipboard aerosol sources to the ocean. *Global Biogeochem. Cycles* **2013**, *27*, 1−10.

(7) Chuang, P. Y.; Duvall, R. M.; Shafer, M. M.; Schauer, J. J. The origin of water soluble particulate iron in the Asian atmospheric outflow. *Geophys. Res. Lett.* **2005**, *32*, L07813.

(8) Sholkovitz, E. R.; Sedwick, P. N.; Church, T. M. Influence of anthropogenic combustion emissions on the deposition of soluble aerosol iron to the ocean: Empirical estimates for island sites in the North Atlantic. *Geochim. Cosmochim. Acta* **2009**, *73*, 3981−4003.

(9) Paris, R.; Desboeufs, K. V.; Formenti, P.; Nava, S.; Chou, C. Chemical characterisation of iron in dust and biomass burning aerosols during AMMA-SOP0/DABEX: Implication for iron solubility. *Atmos. Chem. Phys.* **2010**, *10*, 4273−4282.

(10) Oakes, M.; Ingall, E. D.; Lai, B.; Shafer, M. M.; Hays, M. D.; Liu, Z. G.; Russell, A. G.; Weber, R. J. Iron solubility related to particle sulphur content in source emission and ambient fine particles. *Environ. Sci. Technol.* **2012**, *46*, 6637−6644.

(11) Takahashi, Y.; Furukawa, T.; Kanai, Y.; Uematsu, M.; Zheng, G.; Marcus, M. A. Seasonal changes in Fe species and soluble Fe concentration in the atmosphere in the Northwest Pacific region based on the analysis of aerosols collected in Tsukuba, Japan. *Atmos. Chem. Phys.* **2013**, *13*, 7695−7710.

(12) Wozniak, A. S.; Shelley, R. U.; Sleighter, R. L.; Abdulla, H. A. N.; Morton, P. L.; Landing, W. M.; Hatcher, P. G. Relationships among aerosol water soluble organic matter, iron and aluminum in European, North African, and Marine air masses from the 2010 US GEOTRACES cruise. *Mar. Chem.* **2013**, *153*, 24−33.

(13) Schroth, A. W.; Crusius, J.; Sholkovitz, E. R.; Bostick, B. C. Iron solubility driven by speciation in dust sources to the ocean. *Nat. Geosci.* **2009**, 337−340.

(14) Chen, H.; Laskin, A.; Baltrusaitis, J.; Gorski, C. A.; Scherer, M. M.; Grassian, V. H. Coal fly ash as a source of iron in atmospheric dust. *Environ. Sci. Technol.* **2012**, *46* (4), 2112−2120.

(15) Fu, H.; Lin, J.; Shang, G.; Dong, W.; Grassian, V. H.; Carmichael, G. R.; Li, Y.; Chen, J. Solubility of iron from combustion source particles in acidic media linked to iron speciation. *Environ. Sci. Technol.* **2012**, *46* (20), 11119−11127.

(16) Chen, H.; Grassian, V. H. Iron dissolution of dust source materials during simulated acidic processing: The effect of sulfuric, acetic, and oxalic acids. *Environ. Sci. Technol.* **2013**, *47*, 10312−10321.

(17) Ito, A.; Xu, L. Response of acid mobilization of iron-containing mineral dust to improvement of air quality projected in the future. *Atmos. Chem. Phys.* **2014**, *14*, 3441−3459.

(18) Ito, A.; Feng, Y. Role of dust alkalinity in acid mobilization of iron. *Atmos. Chem. Phys.* **2010**, *10*, 9237−9250.

(19) Ito, A.; Kok, J.; Feng, Y.; Penner, J. E. Does a theoretical estimation of the dust size distribution at emission suggest more bioavailable iron deposition? *Geophys. Res. Lett.* **2012**, *39*, L05807.

(20) Lin, G.; Sillman, S.; Penner, J. E.; Ito, A. Global modeling of SOA: The use of different mechanisms for aqueous phase formation. *Atmos. Chem. Phys.* **2014**, *14*, 5451−5475.

(21) Ito, A.; Lin, G.; Penner, J. E. Global modeling study of soluble organic nitrogen from open biomass burning. *Atmos. Environ.* **2015**, DOI: 10.1016/j.atmosenv.2015.01.031.

(22) Zhang, Y.; Kallay, N.; Matijević, E. Interactions of metal hydrous oxides with chelating agents. 7. Hematite-oxalic acid and -citric acid systems. *Langmuir* **1985**, *1*, 201−206.

(23) Hamer, M.; Graham, R.; Amrhein, C.; Bozhilov, K. Dissolution of ripidolite (Mg, Fe-chlorite) in organic and inorganic acid solutions. *Soil Sci. Soc. Am. J.* **2003**, *67* (2), 654−661.

(24) Lanzl, C. A.; Baltrusaitis, J.; Cwienty, D. M. Dissolution of hematite nanoparticle aggregates: Influence of primary particle size, dissolution mechamism, and solution pH. *Langmuir* **2012**, *28*, 15797−15808.

(25) Lasaga, A. C.; Soler, J. M.; Ganor, J.; Burch, T. E.; Nagy, K. L. Chemical-weathering rate laws and global geochemical cycles. *Geochim. Cosmochim. Acta* **1994**, *58* (10), 2361−2386.

(26) Meskhidze, N.; Chameides, W. L.; Nenes, A. Dust and pollution: A recipe for enhanced ocean fertilization? *J. Geophys. Res.* **2005**, *110*, D03301.

(27) Zuo, Y.; Hoigné, J. Formation of hydrogen peroxide and depletion of oxalic acid in atmospheric water by photolysis of iron(III)-oxalato complexes. *Environ. Sci. Technol.* **1992**, *26*, 1014−1022.

(28) Rotman, D. A.; Atherton, C. S.; Bergmann, D. J.; Cameron-Smith, P. J.; Chuang, C. C.; Connell, P. S.; Dignon, J. E.; Franz, A.; Grant, K. E.; Kinnison, D. E.; Molenkamp, C. R.; Proctor, D. D.; Tannahill, J. R. IMPACT, the LLNL 3-D global atmospheric chemical transport model for the combined troposphere and stratosphere: Model description and analysis of ozone and other trace gases. *J. Geophys. Res.* **2004**, *109*, D04303.

(29) Liu, X. H.; Penner, J. E.; Herzog, M. Global modeling of aerosol dynamics: Model description, evaluation, and interactions between sulfate and nonsulfate aerosols. *J. Geophys. Res.* **2005**, *110*, D18206.

(30) Feng, Y.; Penner, J. E. Global modeling of nitrate and ammonium: Interaction of aerosols and tropospheric chemistry. *J. Geophys. Res.* **2007**, *112*, D01304.

(31) Ito, A.; Sillman, S.; Penner, J. E. Effects of additional nonmethane volatile organic compounds, organic nitrates, and direct

DOI: 10.1021/acs.estlett.5b00007
Environ. Sci. Technol. Lett. 2015, 2, 70−75

emissions of oxygenated organic species on global tropospheric chemistry. *J. Geophys. Res.* **2007**, *112*, D06309.
(32) Xu, L.; Penner, J. Global simulations of nitrate and ammonium aerosols and their radiative effects. *Atmos. Chem. Phys.* **2012**, *12* (20), 9479−9504.
(33) Brandt, F.; Bosbach, D.; Krawczyk-Bärsch, E.; Arnold, T.; Bernhard, G. Chlorite dissolution in the acid pH-range: A combined microscopic and macroscopic approach. *Geochim. Cosmochim. Acta* **2003**, *67*, 1451−1461.
(34) Furukawa, T.; Takahashi, Y. Oxalate metal complexes in aerosol particles: Implications for the hygroscopicity of oxalate-containing particles. *Atmos. Chem. Phys.* **2011**, *11*, 4289−4301.
(35) Kumar, A.; Sarin, M. M. Aerosol iron solubility in semi-arid region: Temporal trend and impact of anthropogenic sources. *Tellus* **2010**, *62B*, 125−132.
(36) Johnson, M. S.; Meskhidze, N. Atmospheric dissolved iron deposition to the global oceans: Effects of oxalate-promoted Fe dissolution, photochemical redox cycling, and dust mineralogy. *Geosci. Model Dev.* **2013**, *6*, 1137−1155.
(37) Takahama, S.; Gilardoni, S.; Russell, L. M. Single-particle oxidation state and morphology of atmospheric iron aerosols. *J. Geophys. Res.* **2008**, *113*, D22202.
(38) Fishwick, M. P.; Sedwick, P. N.; Lohan, M. C.; Worsfold, P. J.; Buck, K. N.; Church, T. M.; Ussher, S. J. The impact of changing surface ocean conditions on the dissolution of aerosol iron. *Global Biogeochem. Cycles* **2014**, *28*, 1235−1250.
(39) Kieber, R. J.; Hardison, D. R.; Whitehead, R. F.; Willey, J. D. Photochemical production of Fe(II) in rainwater. *Environ. Sci. Technol.* **2003**, *37*, 4610−4616.
(40) Cheize, M.; Sarthou, G.; Croot, P. L.; Bucciarelli, E.; Baudoux, A.-C.; Baker, A. R. Iron organic speciation determination in rainwater using cathodic stripping voltametry. *Anal. Chim. Acta* **2012**, *736*, 45−54.

DOI: 10.1021/acs.estlett.5b00007
Environ. Sci. Technol. Lett. 2015, 2, 70−75